Structural dynamics of two-dimensional charge-density waves in CeTe_{3} investigated by ultrafast electron crystallography

Tzong-Ru T. Han, Zhensheng Tao, Subhendra D. Mahanti, Kiseok Chang, Chong-Yu Ruan, Christos D. Malliakas, and Mercouri G. Kanatzidis

Phys. Rev. B **86**, 075145 — Published 27 August 2012

DOI: 10.1103/PhysRevB.86.075145

Structural dynamics of 2D charge density waves in $CeTe_3$ investigated by ultrafast electron crystallography

Tzong-Ru T. Han, Zhensheng Tao, Subhendra D. Mahanti, Kiseok Chang, and Chong-Yu Ruan*
Physics and Astronomy Department, Michigan State University, East Lansing, Michigan 48824

Christos D. Malliakas and Mercouri G. Kanatzidis
Department of Chemistry, Northwestern University, Evanston, IL 60208

The electron-phonon mechanism that gives rise to various charge-ordered systems is often controversial because of the cooperative nature of the transformation and that the structural aspect of the transformation is generally poorly understood. Using femtosecond electron crystallography, we reveal a two-step (≈400 fs and 3.3 ps) suppression of the structural order parameter of a 2D charge density wave (CDW) that clearly decouples from its electronic counterpart following fs optical quenching. Through atomic fluctuational analysis on Bragg reflections and satellite features, we identify important momentum-dependent electron-phonon couplings appearing on both timescales that can be related to interactions between the unidirectional CDW collective modes, the lattice phonons, and the perturbed electronic subsystem. We show that the characteristic timescales of these couplings and relative fluctuational amplitudes as characterized by fs crystallography jointly determine the cooperativity between the electronic and structural subsystems and from this it is possible to elucidate the underlying mechanism of the charge-ordered system.

PACS numbers: 71.45.Lr, 61.50.Ks, 63.20.kd, 06.60.Jn

I. INTRODUCTION

The coexistence of phases through complex couplings between different degrees of freedom (spin, charge, lattice, orbital) is a hallmark of complex materials with emergent properties such as charge density wave (CDW), superconductivity, and colossal magnetoresistivity[1]. In particular, CDW is predicted to form in highly anisotropic systems where long-range charge ordering and periodic lattice distortion are strongly coupled[2–4], driven by instabilities originated in either the electronic (Mott)[5] or phononic (Peierls)[2] subsystems. Recent femtosecond spectroscopy-based pump-probe techniques offered real-time characterizations of nonequilibrium dynamics in different electron-phonon systems[6–16], but their properties cannot be conclusively determined without direct structural resolution to map out the corresponding ionic responses. Using femtosecond electron crystallography we provide a complementary view from the ultrafast structural evolution of $CeTe_3$, exploiting its elegant 2D weakly correlated feature, serving as an ideal system to understand the inherent symmetry breaking phase transition in strongly coupled electron-phonon system.

An outstanding puzzle emerging from earlier ultrafast spectroscopic studies of CDW materials is the identification of a sub-ps partial recovery of electronic ordering following optical quenching[10–16] – seemingly independent of the perceived underpinning mechanism. This intriguing universality might be associated with the lattice being frozen in its modulated state in the sub-ps timescale[13, 16, 17], but there has been no direct proof to this hypothesis. A recent ultrafast electron diffraction study of CDW in a correlated 1T-TaS_2 system[18] reported a contrasting cooperative suppression of the structural and the electronic order parameters that appears on the sub-ps timescale[19]. This singular ultrafast electron diffraction study showed that the rapid recovery of charge ordering might be directly driven by strong electron-phonon coupling in a strongly correlated system[19, 20]. Yet to shed light on the long-standing puzzle additional direct structural studies of charge density waves, preferably in systems without strong correlation effects, are needed.

In the fs electron crystallography study of $CeTe_3$, we reveal a two-step (≈400 fs and 3.3 ps) suppression of the CDW structural order parameter that clearly decouples from its electronic counterpart following fs optical quenching. Moreover, we also observe clear evidences of strong electron-phonon couplings operating on both timescales, which point out an important fact that the order parameter evolutions represent only a subset of changes. By carefully mapping out the correlations between the order parameter and CDW-related atomic fluctuation, we show that the phase transition of the 2D CDW in $CeTe_3$ is primarily phononically driven. However, a joint consideration of the couplings between the lattice phonons, the uniaxial CDW collective modes, and the perturbed electronic subsystems is required to account for the various novel structural dynamics features that are characteristic of a Peierls-distorted 2D CDW in $CeTe_3$.

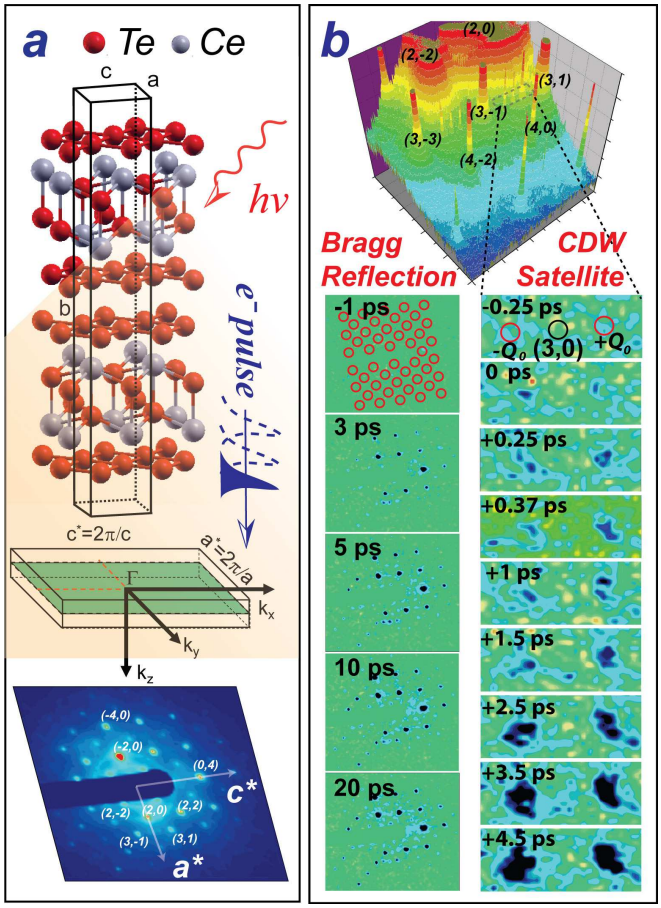

FIG. 1: (Color online) (a) Crystal structure of $CeTe_3$ with the corresponding reciprocal lattice. The lattice constant a=4.384Å, b=26.05Å, c=4.403Å[21]. The femtosecond (fs) electron pulse is directed along b-axis, producing a transmission diffraction pattern. The fs laser pulses illuminate the sample area at 45° angle. (b) The top panel shows the 3D diffraction intensity map, where the CDW satellites are located at $3\mathbf{a}^*\pm\mathbf{Q}_0$ in the dashed region. The lower panels show the temporal evolution of ultrafast electron crystallography patterns subtracted by the equilibrium state pattern taken before fs laser excitation (t<0) to highlight the induced changes, showing ps sequences for Bragg reflections, and fs-to-ps sequences in scale-up view of the region near CDW satellites.

II. EXPERIMENTAL METHODS

The $CeTe_3$[21–24] layered compound has a unit cell composed of a metallic planar net of Te sandwiched by the insulating corrugated double layers of CeTe[21, 24], as depicted in Fig. 1a. The charge density waves reside within the 2D square Te net and cause a uniaxial periodic lattice distortion at wave vector $\mathbf{Q}_0$=0.28$\mathbf{c}^*$, which can be characterized by transmissive diffraction as satellites[21, 24, 25] distributed on the sides of main Bragg reflections, indexed as (m,n) based on reciprocal wave vector $\mathbf{q}$=m$\mathbf{a}^*$+n$\mathbf{c}^*$. Unlike 1T-TaS_2, the unidirectional p-wave CDW in $CeTe_3$ breaks the underlying square lattice symmetry and has a weak electron correlation, which present some unique advantages in de-convoluting the CDW-specific structural effects from the uncorrelated 2D lattice dynamics following optical quenching. Here, the structural dynamics of a single-crystal $CeTe_3$ film (40±10 nm) is investigated by ultrafast electron crystallography(UEC) technique[26, 27]. To quench the charge orderings, we used an intense 50 femtosecond (fs) infrared (λ=800nm) laser pulse at 1 kHz to excite electrons across the CDW gap($\Delta \approx 0.4$eV)[22] ranging from 1 to 7 mJ/cm^2. The anisotropic electron-phonon coupling, essential to the formation of charge density waves and the quasi-1D Peierls-distorted structure, is present in the dynamical asymmetric responses along the **c**-axis. Meanwhile, the non-specific phonon excitations from interaction with the hot carriers excited by laser pulses can be examined from the orthogonal Bragg reflections as comparison groups. However, to examine these central dynamical features from individual reflections extremely high signal-to-noise ratio is required as the satellite features that encode the mesoscopically ordered density waves structure are 2-3 orders of magnitude weaker than the nearby Bragg reflections. We employed extremely large numbers of pump-probe cycles ($\geq 6\times10^6$) to accumulate $\sim10^3$ electrons and over 10^6 electrons for individual satellites and Bragg reflections in each dynamical frame. The respective changes, as shown in the lower panels in Fig. 1b, are highlighted in the diffraction difference images. The asymmetric and noncooperative characters of the transition can be readily seen on the sub-ps timescale where only the satellite reflections exhibit intensive changes, whereas the orthogonal Bragg reflections, such as (3,0), are largely unperturbed, which are quite different from 1T-TaS_2 system[19].

III. RESULTS AND ANALYSIS

We single out an orthogonal pair of Bragg reflections (-4,0) and (0,4) to investigate the phononic responses imposed on the 2D lattice by the carriers and CDW excitations. The upper panel of Fig. 2 depicts these relative changes at three laser fluencies (F=2.43, 4.62, 7.30 mJ/cm^2). Meanwhile, the evolutions of the CDW satellite intensity under the same conditions are shown in the lower panel for comparison. For the Bragg reflections, the changes along the CDW axis [(0,4)] are consistently larger than non-CDW-related ones [(-4,0)], which clearly indicates an elevated lattice fluctuation accompanying the melting of charge density waves. In contrast, the phononic signatures encoded in the (-4,0) intensities are deferred by ≈1.5 ps across all fluences. This characteristic deference can be identified also in the (0,4) as a perturbation over an otherwise undeferred exponential decay that commences at time zero, making such deferred re-

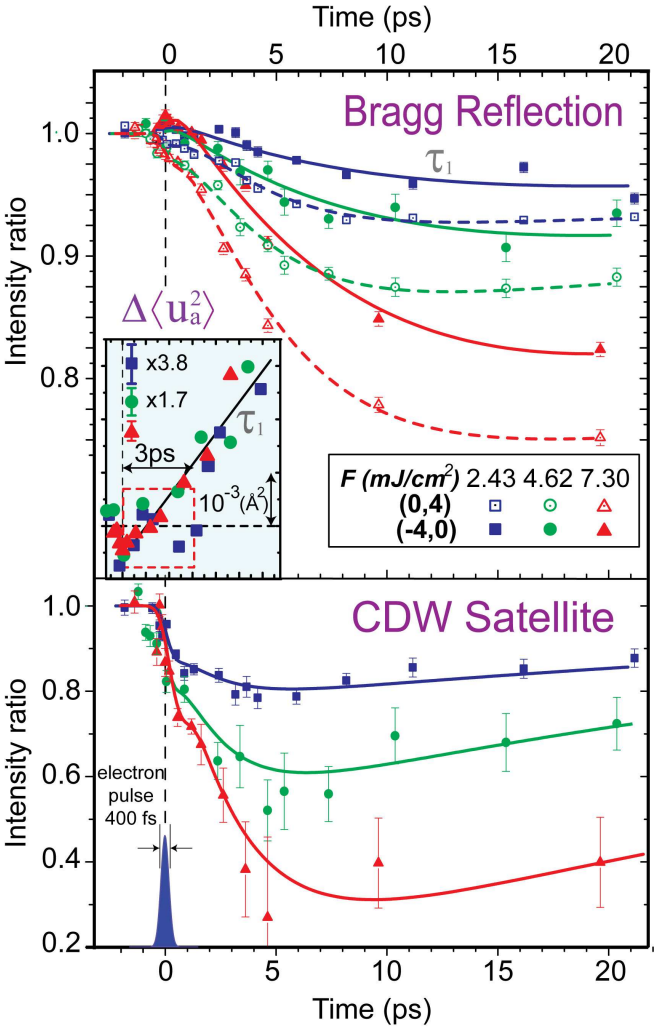

FIG. 2: (Color Online) (a) The normalized Bragg reflection intensity at $\mathbf{q}$=-4$\mathbf{a}$* and 4$\mathbf{c}$* under three diffraction laser fluencies, F=2.43, 4.62, and 7.30 mJ/cm^2. The associated error bars are based on electron counting statistics. Inset shows the early time evolution of the thermal displacement variance ($\Delta\langle u_a^2\rangle$) deduced from (-4,0), in which low fluence data are linearly scaled up to compare with data at F=7.30 mJ/cm^2. (b) The normalized satellite intensity at $\mathbf{q}_{CDW}$=3$\mathbf{a}$*+$\mathbf{Q}_0$, showing a nonscalable two-step suppression feature.

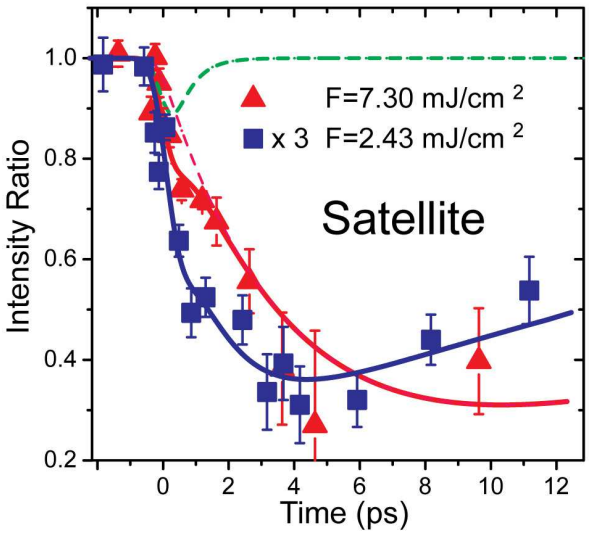

FIG. 3: (Color Online) The scaled-up view of satellite intensity at early times showing two-step suppression, along with the two-component fits. The data from F=2.43 mJ/cm^2 are multiplied by 3 to compare with data from F=7.30 mJ/cm^2. The fast and slow channels for F=7.30 mJ/cm^2 are shown in dashed lines. The error bars are calculated based on the counting statistics.

sponse a signature of non-CDW related electron-phonon coupling over 2D lattice. Interestingly, the large asymmetry between the orthogonal set of Bragg reflections persists for more than 20 ps, representing that the two excited phonon manifolds, one coupled with CDW and the other generated from 2D electronic relaxations, are highly isolated from each other.

We now examine the corresponding collective state evolution from the CDW satellites depicted in the lower panel in Fig. 2, which shows clearly two-step features not consistent with the lattice dynamics. The distinction can be most clearly investigated from the non-scalability in these dynamics, as shown in Fig. 3. At fluence F=2.43 mJ/cm^2 up to 80% of the maximum suppression of satellite intensity is achieved within 1 ps; whereas at F=7.30 mJ/cm^2 it takes 3 ps to do the same. Such suppressions are non-exponential and can be satisfactorily fitted by two independent exponential rise/decay channels (dashed lines in Fig. 3). We examine the fluence-dependent behavior further by singling out each channel. The fast channel, denoted as S_1^ϕ, extracted from the fits and shown in Fig. 4a, has a resolution-limited[26, 28] responses with a τ_s=350 fs and τ_r=570 fs representing a sub-ps partial suppression and recovery of the structural order parameter that saturates around F$_c$ ≈3.8 mJ/cm^2 (inset). In contrast, the ps dynamics, denoted as S_1^A, that ultimately leads to melting has an amplitude-dependent suppression timescale but its amplitude is linear with the fluence up to F=7 mJ/cm^2. It is intriguing that while the fast dynamics identified in the structural order parameter is temporarily strongly correlated to the charge melting and recovery widely seen in the recent spectroscopy-based studies[10–17], the fluence-dependent ps dynamics identified here has not been reported previously and may represent the characteristic features pertaining to the structural melting of a Peierls-distorted 2D CDW.

Because of the distinctive 1D and 2D lattice fluctuational features and the well isolated satellite dynamics, we can extract quantitatively from these observations the phonons and CDW dynamics using the CDW structure

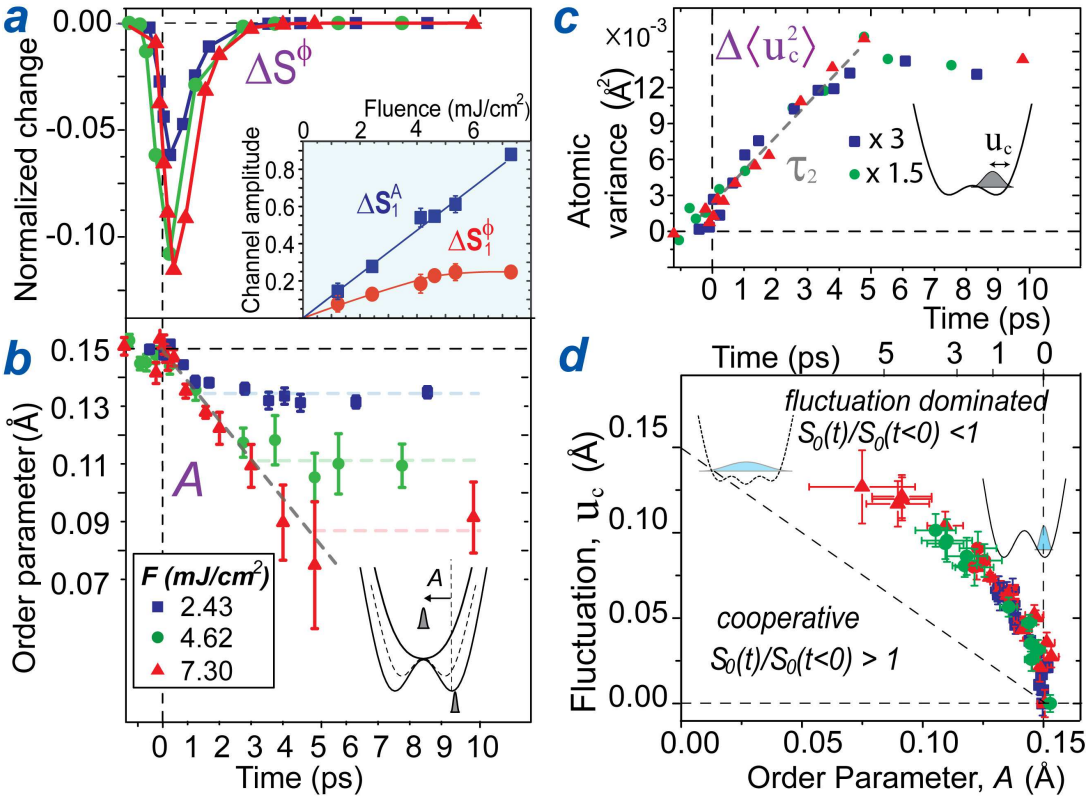

FIG. 4: (Color Online) (a) The fast component of satellite suppression (ΔS_1^{ϕ}), showing an extremely fast decay and recovery. The inset shows the amplitude of the fast (ΔS_1^{ϕ}) and slow (ΔS_1^{A}) components extracted from fitting. A saturation of ΔS_1^{ϕ} at around F=3.8 mJ/cm^2 is identified. (b) The temporal evolution of structural order parameter (A). The reduction of A represents symmetry recovery as described by the CDW potential evolving from double well to single well. (c) The CDW collective mode fluctuational variance ($\Delta\langle u_c^2\rangle$), deduced from anisotropy analysis. (d) CDW fluctuation amplitude (u_c) - order parameter (A) correlation plot.

factor, previously derived by Giulani and Overhauser[29]:

$$S_n(\mathbf{q}) = \sum_{\mathbf{q}} \sum_{n=-\infty}^{\infty} \delta[\mathbf{q} - (\mathbf{G} + n\mathbf{Q})] J_n^2(\mathbf{q}\cdot\mathbf{A}) F_n^{\phi} F_n^{A} F^{P}(\mathbf{q}), \quad (1)$$

where $\mathbf{G}$ is the reciprocal lattice vector, $\mathbf{q}$ is the electron scattering wave vector. $\mathbf{Q}$ and $\mathbf{A}$ describe the wave vector and the distortion amplitude of CDW. J_n is the Bessel function of the first kind of order n, which determines the maximum intensity of satellite ($n = 1$) and Bragg ($n = 0$) reflections. F_n^{ϕ} and F_n^{A} are the collective mode attenuation factors induced by phase and amplitude fluctuations (δ_{ϕ} and δ_A, respectively) within the CDW collective state: $F_n^{\phi} = exp(-2n^2 W_{\phi}(T))$ where $W_{\phi}(T)=1/2\langle\delta_{\phi}^2\rangle$, and $F_n^{A} = exp(-2(n^2 - |n|)W_A(T))$ where $W_A(T)=1/2\langle\delta_A^2\rangle$. Finally, $F^P = exp(-\langle(\mathbf{q}\cdot\mathbf{u})^2\rangle)$ is the Debye-Waller factor induced by atomic lattice fluctuation $\mathbf{u}$. Some important observations can be made. Firstly, we recognize that the satellites and Bragg intensities are jointly influenced by CDW order parameter A because for small A $J_1(A)$ and $J_0(A)$ anticorrelates with each other. Secondly, the amplitude fluctuations play no role in the satellite suppression(F_1^A=1), however, amplitude fluctuations can couple strongly to soft modes near $\mathbf{Q}_0$[11, 30–32] (Kohn anomaly) and directly contribute to the decay of Bragg reflections along the $\mathbf{c}$-axis. Thirdly, utilizing the symmetry pertaining to the hot-electron-relaxation-mediated 2D lattice fluctuations, the CDW-induced uniaxial fluctuations can be deduced from the anisotropy ratio $\gamma = S_0(4\mathbf{c}^*)/S_0(-4\mathbf{a}^*)$, in the case of Fig.2, where $\Delta\langle u_c^2\rangle = -ln[(\gamma(t)/J_0(t)]/8|\mathbf{c}^*|^2$. Lastly, the decrease of satellite intensity can either describe the actual suppression of the order parameter [$J_1(A)$ term], or merely a reflection of temporal phase fluctuations (F_1^{ϕ} term) without reducing A.

Given that we can differentiate the non-CDW-related contribution in the lattice responses, we can now calculate the CDW-related structural order parameter (A) and amplitude fluctuations (u_c) from our experimental results following the Giulani-Overhauser formalism, as shown in the panels b and c in Fig. 4 respectively. In calculating A, we have excluded the fast channel, which we attribute to a phase-related decay induced by charge melting. This exclusion yields a clean result showing linear

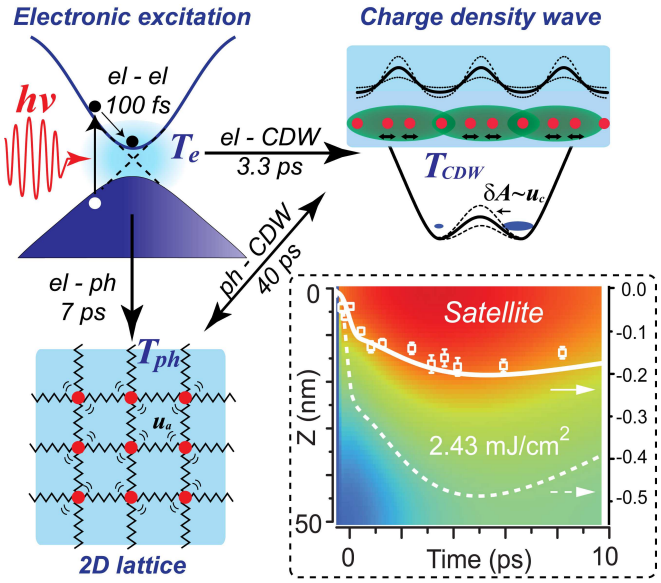

FIG. 5: (Color Online) Conceptual framework of the three-temperature model (TTM). The photoinduced CDW dynamics is initiated by the generation of hot carriers through above the CDW gap photoexcitation by intense laser pulse ($h\nu$). The photo-generated hot carriers quickly equilibrate with the unexcited carries at ≈ 100 fs timescale. The decay of stored optical energy in the electronic manifold into the lattice counterparts is via three coupling channels: the coupling between the hot carriers and the 2D lattice phonons (el-ph coupling, τ_1), the coupling between the hot carriers and the CDW collective modes (el-CDW coupling, τ_2), and the coupling between the 2D lattice phonons and the CDW collective modes (ph-CDW coupling, τ_3). The lower right panel describes the TTM simulation of the CDW suppression using τ_1=7ps, τ_2=3.3ps, and τ_3=40ps as the coupling time constants, considering the laser penetration depth along the z-axis. The dashed line shows the TTM simulation at the surface (z=0), and the solid line shows the simulation averaged across the sample slab from 0 to 50 nm, compared with the data points at fluence F=2.43 mJ/cm^2.

suppression of order parameter, ranging from 1 to 4 ps, that increases with the excitation laser fluence (F). The dynamical slowdown demonstrated in the suppression of the structural order parameter can be understood as inherent to a second-order phase transition in which the softening of the lattice potential at Q_0 (Kohn anomaly) drives the phase transition[33]. This phononic origin of the phase transition is clearly seen in the corresponding increase of fluctuational amplitude u_c as the order parameter A is quenched as indicated in Figs. 4b&c. In a more direct comparison, we combine the information from Figs. 4b&c to construct a fluctuation landscape in an order parameter – atomic fluctuation correlation plot as shown in Fig. 4d, where the CDW melting following an arc trajectory that starts from the equilibrium state where the distortion as described by the separation of the double well potential is A_0 ≈0.15Å[34]. The fact that the CDW fluctuation amplitude reaches a similar value $u_c \approx 0.15\AA$ when the double well potential is quenched into a symmetric state represents a rather unique situation that the potential well is literally flattened in the high-temperature CDW state.

The origin of the ultrafast phase fluctuation might be attributed to the reduction of the long-range coherence of the CDW collective state. Electronically induced fragmentation has been seen previously in nanoparticles under surface plasmon resonance excitation[35] without significantly transferring energy into the lattice sub-system, as evidenced by a rapid nonthermal recovery in the structure factor following the electronic recovery. The presence of this electronically induced fragmentation of CDW is further supported by the observation of topological defects in the optical reflectivity signals as a first step for the recovery of CDW in the electronic subsystem[12]. An alternative explanation is that the partial suppression of the satellite intensity is directly the scattering contribution from the valence part of coulomb potential, which is modified by charge quenching. While this explanation does not fundamentally change the nature of decoupling between the electronic and structural order parameters on the sub-ps timescale, our analysis based on the electronic form factor contribution indicates that direct charge scattering is less than 2%[36] of the ionic counterpart at the scattering vector of the satellite used in our analysis ($q_{CDW} \approx 4.7\AA^{-1}$), which is inconsistent with the up to 25% change seen in the satellite intensity.

Another novel aspect of 2D CDW melting, not identified by optical studies, is the momentary stiffening of the lattice that is behind the deference of the suppression of Bragg reflections described earlier. This effect can be quantified by calculating Debye-Waller factor on (-4,0), as representative of the inherent lattice response to the fs heating of 2D electron gas. A narrowing of fluctuational variance occurs nearly instantaneously as shown in the inset of Fig. 2. This narrowing can be translated into a stiffening in the mean atomic potential, which has been observed in graphite[37] under similar optical quenching. The mechanism for the stiffening phenomena has been attributed to the inability for excited electrons to adiabatically follow the lattice dynamics in the low-dimensional systems by a density functional theory with nonadiabatic implementation[37]. As in graphite, this stiffening phenomenon lasts just over the hot electron lifetime (≈ 1ps)[11], after which the 2D lattice might be heated first through optical phonon emission (at $\mathbf{q}$≈0) and followed by the ensuing phonon cascades to reach thermalization, characterized by the baseline rise of $\Delta\langle u_a^2\rangle$ (inset in Fig. 2a) on a ≈ 7 ps (τ_1) timescale.

Summing up, we have observed a sequence of events that can be traced to the interplays between the uniaxial CDW-related softmodes, the lattice phonons, and the perturbed electronic subsystem. We can use a phe-

nomenological three-temperature model (TTM) to capture the asynchronous electronic and structural melting of the CDWs, driven respectively by the hot electrons and collective modes. In the TTM framework as described in Fig. 5, the spatial and temporal evolutions of the energy stored within the photoexcited electrons, CDW collective modes, and lattice phonons (whose temperatures are denoted as T_e, T_{CDW}, T_{ph}) can be modelled based on the observed coupling time constants (τ_1,τ_2,τ_3)[38]. We also consider depth inhomogeneity in the optical excitation (laser penetration depth d_L=20 nm[39]). The inset of Fig. 5 reports the comparisons and shows a difference between the bulk-averaged dynamics (integrated from 0-50nm) and the corresponding one at the surface (z=0). The coarse-grained through-slab dynamics observed by the transmission ultrafast electron crystallography is more than a factor of 2 less pronounced compared to the surface dynamics, which is relevant to optical and photoemission investigations. Importantly, the critical fluence for electronic suppression, as determined from the departure from linearity in ΔS_1^{ϕ} depicted in the inset of Fig. 4a, is reduced to 1.9±0.4 mJ/cm^2, generally agreeing with the threshold (between 1-2 mJ/cm^2) identified by ultrafast angle-resolved photoemission study of the isostructural $TbTe_3$[11]. Using F_c=1.9 mJ/cm^2, we obtain a critical density E_c=$F_c(1-R)/[d_L \cdot (u.c.v.)]$=0.9±0.2 eV/($u.c.v.$) (R=0.7[39] is the reflectivity, $u.c.v.$ stands for unit cell volume). We can also estimate the mean-field limit of the critical density based on the CDW condensation energy $E_{el} = n(\varepsilon_F)\Delta^2[1/2+ln(2\varepsilon_F/\Delta)]$[2], where Δ=0.4eV is the CDW gap[22], $n(\varepsilon_F)$=1.48 state/eV/($u.c.v.$) is the ungapped density of state near Fermi energy ε_F=3.25eV[40]. The specific agreement between the mean-field value of E_{el}=0.8eV/($u.c.v.$) and the critical density E_c extracted from our experiments supports that the fs partial structural order parameter response is indeed correlated with the disruption of charge ordering.

IV. CONCLUSIONS

We have constructed a noncooperative photoinduced melting picture of 2D CDW in $CeTe_3$ from the fs electron crystallography. We now examine if the dynamical picture painted here can help answer the outstanding issue regarding the universally observed nonthermal rapid partial recovery of charge ordering emerged from the spectroscopy-based measurements[13, 16, 17] and recent fs ultrafast electron diffraction experiment[19, 20]. Clearly, we have established a two-step structural response to the optical quenching of CDW, in which the majority of structural suppression happens on the ps timescale, decoupled from the fs charge melting. This observation is a direct proof that the periodically modulated ionic potential well has not been significantly modified during charge melting, therefore it can facilitate the rapid recovery of the electronic order parameter as proposed by Demsar and coworkers[17]. We believe the separation of structural and electronic order parameters is a result of significant difference in the effective mass in the two subsystems, and the fact that the charge ordering is inherently coupled to the valence electrons that are excited directly by the fs laser pulses. The coupling between the electronic and ionic subsystems can be reestablished as soon as the electronic temperature is reduced to a threshold where stable CDW condensate can exist. However, the cooling of the quasi-particle does not fully depend on the CDW, as the 2D electron-electron and electron-phonon coupling will take place in the process at the quasi-particle levels. Therefore, the timescales of the fast channel are directly related to the quasiparticle dynamics, which has little to do with the specific CDW mechanism. This is supported by the apparent universality of sub-ps recovery of charge ordering from monitoring the electronic channel alone across a spectrum of different CDW systems. Therefore, important distinctions can be best made from the ionic frame through examining the ps structural response following the electronic perturbation of the CDW.

In the CDW with strong electron correlation enhancement, the electron-phonon coupling has been attributed with strong local bonding character[4]. This might be the case in Mott insulator 1T-TaS_2, where the commensurate CDW phase transition near 183K is coupled to a metal-insulator transition and induces a transfer of spectral weight between the inner and outer rings of the 1T-TaS_2 superstructure[4]. As described by the Giulani-Overhauser formalism, the appearance of the cooperativity between CDW satellite and Bragg reflections is strongly influenced by the relative change of the order parameter compared to the atomic fluctuation associated with the phase transition. Therefore, from the high degree of cooperativity between the Bragg reflection and CDW satellite shown in the ultrafast electron diffraction study of 1T-TaS_2[19], it is evident that the charge-transfer-driven phase transition of 1T-TaS_2 has a relative small fluctuation amplitude during the order parameter suppression, and its trajectory should fall into the lower left part of Fig. 4d (J_0 factor dominates over F^P to make $S_0(t)/S_0(t<0)>1$). In contrast, the noncooperative phononic signatures uncovered here for $CeTe_3$ illustrate an extreme case of fluctuation-dominated phase transition and may very well represent the nonequilibrium dynamics for an entire class of inherently Peierls-distorted electron-phonon systems. Thus, we have demonstrated that femtosecond electron crystallography as a powerful approach to tackle long standing issues regarding the nature of electron-phonon couplings in 2D charge ordered systems. Future theoretical modeling taking into account the anisotropic momentum-dependent electron-phonon coupling and experiments on related CDW systems in

different coupling scenarios and energies will further elucidate the fundamental physics across a myriad of structurally correlated electronic phase transition phenomena in complex materials.

V. ACKNOWLEDGEMENT

We acknowledge A. Baczewski, M.-S. Lee, I.R. Fisher, D. Mihailovic for critical discussions. Work at Michigan State University was supported by Department of Energy under grant DE-FG02-06ER46309. K.C. acknowledges support from National Science Foundation under grant DMR 0703904. Materials synthesis was supported by National Science Foundation under grant DMR 0702911.

* Corresponding author: ruan@pa.msu.edu

[1] E. Dagotto, Science **309**, 257 (2005).
[2] G. Gruner, Density Waves in Solids (vol. 89 of Frontiers in Physics, Addison-Wesley, Reading, MA 1994).
[3] M.D. Johannes, I.I. Mazin, Phys. Rev. B **77**, 165135 (2008).
[4] K. Rossnagel, J. Phys.: Condens. Matter **23**, 213001 (2011).
[5] J.A. Wilson, F.J. Di Salvo, S. Mahajan, Adv. Phys. **50**, 1171 (2001).
[6] T. Ogasawara, T. Kimura, T. Ishikawa, M. Kuwata-Gonokami, Y. Tokura, Phys. Rev. B **63**, 113105 (2001).
[7] A. Cavalleri, Th. Dekorsy, H.H.W. Chong, J.C. Kieffer, R.W. Schoenlein, Phys. Rev. B **70**, 161102(R) (2004).
[8] C. Kubler, H. Ehrke, R. Huber, R. Lopez, A. Halabica, R. F. Haglund, Jr., A. Leitenstorfer, Phys. Rev. Lett. **99**, 116401 (2007).
[9] P. Kusar, V. V. Kabanov, J. Demsar, T. Mertelj, S. Sugai, D. Mihailovic, Phys. Rev. Lett. **101**, 227001 (2008).
[10] J. Demsar, K. Biljakovic, D. Mihailovic, Phys. Rev. Lett. **83**, 800 (1999).
[11] F. Schmitt, P.S. Kirchmann, U. Bovensiepen, R.G. Moore, L. Rettig, M. Krenz, J.-H. Chu, N. Ru, L. Perfetti, D.H. Lu, M. Wolf, I.R. Fisher, Z.-X. Shen, Science **321**, 1649 (2008).
[12] R. Yusupov, T. Mertelj, V.V. Kabanov, S. Brazovskii, P. Kusar, J.-H. Chu, I.R. Fisher, D. Mihailovic, Nature Phys. **6**, 681 (2010).
[13] L. Perfetti, P. A. Loukakos, M. Lisowski, U. Bovensiepen, H. Berger, S. Biermann, P. S. Cornaglia, A. Georges, M. Wolf, Phys. Rev. Lett. **97**, 067402 (2006).
[14] K. Kimura, H. Matsuzaki, S. Takaishi, M. Yamashita, H. Okamoto, Phys. Rev. B **79**, 075116 (2009).
[15] T. Rohwer, S. Hellmann, M. Wiesenmayer, C. Sohrt, A. Stange, B. Slomski, A. Carr, Y. Liu, L.M. Avila, M. Kallne, S. Mathias, L. Kipp, K. Rossnagel, M. Bauer, Nature **471**, 490 (2011).
[16] S. Hellmann, M. Beye, C. Sohrt, T. Rohwer, F. Sorgenfrei, H. Redlin, M. Kallane, M. Marczynski-Buhlow, F. Hennies, M. Bauer, A. Fohlisch, L. Kipp, W. Wurth, K. Rossnagel, Phys. Rev. Lett. **105**, 187401 (2010).
[17] A. Tomeljak, H. Schafer, D. Stadter, M. Beyer, K. Biljakovic, J. Demsar, Phys. Rev. Lett. **102**, 066404 (2009).
[18] P. Fazekas, E. Tosatti, Phil. Mag. B **39**, 229 (1979).
[19] M. Eichberger, H. Schfer, M. Krumova, M. Beyer, J. Demsar, H. Berger, G. Moriena, G. Sciaini, R.J.D. Miller, Nature **468**, 799 (2010).
[20] J.D. Lee, P. Moon, M. Hase, Phys. Rev. B **84**, 195109 (2011).
[21] C. Malliakas, S.J.L. Billinge, H.J. Kim, M.G. Kanatzidis, J. Am. Chem. Soc. **127**, 6510 (2005).
[22] V. Brouet, W.L. Yang, X.J. Zhou, Z. Hussain, N. Ru, K.Y. Shin, I.R. Fisher, Z.X. Shen, Phys. Rev. Lett. **93**, 126405 (2004).
[23] H. Komoda, T. Sato, S. Souma, T. Takahashi, Y. Ito, K. Suzuki, Phys. Rev. B **70**, 195101 (2004).
[24] E. DiMasi, M.C. Aronson,J.F. Mansfield, B. Foran, S. Lee, Phys. Rev. B **52**, 14516 (1995).
[25] N. Ru, C.L. Condron, G.Y. Margulis, K.Y. Shin, J. Laverock, S.B. Dugdale, M.F. Toney, I.R. Fisher, Phys. Rev. B. **77**, 035114 (2008).
[26] C-Y. Ruan, Y. Murooka, R.K. Raman, R.A. Murdick, R.J. Worhatch, A. Pell, Microsc. Microanal. **15**, 323 (2009).
[27] A.H. Zewail, Annu. Rev. Phys. Chem. **57**, 65 (2006).
[28] Z. Tao, H. Zhang, P.M. Duxbury, M. Berz, C.-Y. Ruan, J. Appl. Phys. **111**, 044316 (2012).
[29] G.F. Giuliani, A.W. Overhauser, Phys. Rev. B **23**, 3737 (1981).
[30] R.V. Yusupov, T. Mertelj, J.-H. Chu, I.R. Fisher, D. Mihailovic, Phys. Rev. Lett. **101**, 246402 (2008).
[31] M. Lavagnini, M. Baldini, A. Sacchetti, D. Di Castro, B. Delley, R. Monnier, J.-H. Chu, N. Ru, I.R. Fisher, P. Postorino, L. Degiorgi, Phys. Rev. B **78**, 201101 (R) (2008).
[32] P. Kusar, T. Mertelj, V.V. Kabanov, J.-H. Chu, I.R. Fisher, H. Berger, L. Forro, D. Mihailovic, Phys. Rev. B **83**, 035104 (2011).
[33] S.-K. Chan, V. Heine, J. Phys. F: Metal Phys. **3**, 795 (1973).
[34] H.J. Kim, C.D. Malliakas, A.T. Tomic, S.H. Tessmer, M.G. Kanatzidis, S.J.L. Billinge, Phys. Rev. Lett. **96**, 226401 (2006).
[35] R.K. Raman, R.A. Murdick, R.J. Worhatch, Y. Murooka, S.D. Mahanti, T.-R. T. Han, C.-Y. Ruan, Phys. Rev. Lett. **104**, 123401 (2010).
[36] J.-C. Zheng, Y. Zhu, L. Wu, J.W. Davenport, J. Appl. Cryst. **38**, 648 (2005).
[37] K. Ishioka, M. Hase, M. Kitajima, L. Wirtz, A. Rubio, H. Petek, Phys. Rev. B **77**, 121402(R) (2008).
[38] R.A. Murdick, PhD thesis, Michigan State University (2009). Effective local temperatures and specific heats in the electronic, CDW, and 2D lattice manifolds are described by T_i and C_i, where i=el, CDW, and ph, respectively. We can write the coupling equations $C_i \partial T_i/\partial t = -G_{ij}(T_i - T_j) - G_{ik}(T_i - T_k)$ to describe the energy exchange between the three manifolds, where G_{ij} is the coupling constant between two manifolds. Because of the weak out-of-plane coupling between the excited Te-planes, the energy and charge diffusions along the z-axis can be ignored on the timescale considered here. Informed by the time constants: $\tau(el-CDW)$, $\tau(el-ph)$, and $\tau(ph-CDW)$ obtained in our experiments, we can establish the constraints: $G_{ij}/C_i = \tau_{ij}$ and solve the coupled differential equations iteratively. We find this sim-

ple three-temperature model adequately captures the key features of the space-time evolution of the thermal energy flow in and out of the CDW manifold as comapred to a more sophisticated three-temperature model incorporating the proper z-axis diffusions and the heat capacities associated with each manifold, which will be published elsewhere.

[39] A. Sacchetti, E. Arcangeletti, A. Perucchi, L. Baldassarre, P. Postorino, S. Lupi, N. Ru, I.R. Fisher, L. Degiorgi, Phys. Rev. Lett. **98**, 026401 (2007).

[40] V. Brouet, W.L. Yang, X.J. Zhou, Z. Hussain, R.G. Moore, R. He, D.H. Lu, Z.X. Shen, J. Laverock, S.B. Dugdale, N. Ru, I.R. Fisher, Phys. Rev. B **77**, 235104 (2008).